Dielectric inserts for sensitivity and RF magnetic field enhancement in NMR volume coils

Arnon Neufeld [a], Naftali Landsberg [b], Amir Boag [b,*]

[a] The Wohl Institute for Advanced Imaging, Tel Aviv Sourasky Medical Center, 6 Weizmann Street, Tel Aviv, Israel
[b] School of Electrical Engineering, Tel Aviv University, Tel Aviv 69978, Israel

ABSTRACT

A method for enhancing the signal to noise ratio (SNR) in NMR volume coils is described. By introducing inserts made of low-loss, high dielectric constant material into specific locations in the coil, the SNR can often be enhanced by up to 20%, while B_1 homogeneity is hardly affected. A model for predicting the limit of the SNR improvement is also presented. The model accurately predicts the SNR gain obtained in both numerical simulations and experiment. An experiment was conducted on a mini-MRI system. Experimental results are in very good agreement with the simulations in regard to both SNR improvement and B_1 enhancement in transmission. Inserts made of ultra high dielectric constant materials can be as thin as few millimeters, thus, conveniently fitting into existing coil-sample gaps in volume coils.

© 2009 Elsevier Inc. All rights reserved.

1. Introduction

The performance of an NMR radiofrequency (RF) coil is conventionally assessed based on two key performance merits, namely, the homogeneity of the transverse component of the radiofrequency magnetic field – B_1, and the signal to noise ratio (SNR) obtained by the coil. It is desirable for B_1 to be as homogenous as possible to facilitate the generation of uniform tilt-angles during excitation and for uniform sensitivity during the signal detection. Also, the SNR should be as high as possible since this is the limiting factor for the threshold of detection and in the case of imaging (MRI) also for the resolution, degree of contrast that may be used, and the overall scan time.

By the principle of reciprocity [1], the distribution of B_1 created by a coil during transmission is identical to the sensitivity profile of the same coil during detection. Thus, if B_1 can be enhanced to some degree for a given point in space during transmission, an identical increase in the acquired signal will be measured from the same point during detection. The noise in a volume coil results from the interaction of the RF electric field E with the whole sample, and the noise magnitude depends on the total conductive loss over the whole lossy sample (or biological tissues, in the MRI case) [2,3]. Note that for a volume coil, we assume that the losses in the coil

proper are low in comparison with those in the sample. Thus, to reduce the noise in an NMR experiment we will seek reduction in the electric field inside the sample.

There is a slight difference between calculating the SNR in MRI and in spectroscopy. The main difference, is that while in MRI we might be interested in the SNR of a specific voxel or the *average* SNR, in spectroscopy the SNR depends on the *cumulative* magnetic field at all points, since we collect the emitted energy from the *entire* volume of interest. Therefore, based on Ref. [3], the SNR in spectroscopy can be related to the magnetic and electric fields during transmission in the entire volume of interest:

$$SNR \propto \frac{\int_V B_1(\mathbf{r})\,dv}{\sqrt{\int_V \sigma(\mathbf{r})\,|\mathbf{E}(\mathbf{r})|^2\,dv}} \triangleq IFR \qquad (1)$$

where $B_1(\mathbf{r})$ is the properly polarized component of the magnetic field, V is the volume of the lossy materials with conductivity $\sigma(\mathbf{r})$, and $\mathbf{E}(\mathbf{r})$ is the electric field inside the sample. Here, we define an integrated fields ratio (*IFR*) as a convenient figure of merit for the fields' distribution influence on the SNR. It is important to emphasize that the *IFR* depends not only on the sample's conductivity, electric and magnetic fields, but also on the volume of the sample. This expression is convenient for coil design as it allows one to evaluate how the manipulation of these fields affects the SNR.

The homogeneity of a coil sensitivity (which is dependent on the homogeneity of the B_1 field) can be evaluated using:

$$\text{Homogeneity} \triangleq 1 - \frac{\sigma_B}{\langle |B_1| \rangle} \qquad (2)$$

* Corresponding author. Address: Department of Physical Electronics, School of Electrical Engineering, Faculty of Engineering, Tel-Aviv University, Tel Aviv 69978, Israel. Fax: +972 36 42 3508.
E-mail address: boag@eng.tau.ac.il (A. Boag).
URL: http://www.eng.tau.ac.il/~boag/ (A. Boag).

where σ_B denotes the standard deviation of B_1:

$$\sigma_B = \sqrt{\frac{1}{V} \int_V (|B_1(\mathbf{r})| - \langle |B_1(\mathbf{r})| \rangle)^2 \, dV} \qquad (3)$$

and the average value of the magnetic field is defined by:

$$\langle |B_1| \rangle = \frac{1}{V} \int_V |B_1(\mathbf{r})| \, dv \qquad (4)$$

Here, we use the magnitude of the magnetic field in all of the above equations in order to obtain simpler, real valued results. Note that while the *IFR* and *Homogeneity* are defined for the linear polarization of the coil, these definitions apply also to the case of circular polarization – B_1^+. When going from linear to circular detection the ratio in Eq. (1) remains unaffected, although the SNR is increases by $\sqrt{2}$.

In this work, an attempt is made to improve the ratio between the integrated RF magnetic field and the electric field within the effective scanning region of several spectroscopy coils of various sizes and operating frequencies. This is achieved by using inserts made of dielectric materials. The use of dielectric materials to manipulate B_1 has been discussed by several authors: Foo and coworkers [4] predicted better B_1 homogeneity for shielded volume coils where the dielectric material is placed between the coil and the shield. This configuration was also tested in [5] and was demonstrated to improve the homogeneity and SNR in MRI (but no consequences on spectroscopy were described). Using high dielectric constant material as a shield for the electric field in MRI has been proposed in Ref. [6], but no analysis or results were given. Other studies used asymmetric dielectric loading in order to change the sensitivity profile of B_1 [7,8]. In these works, the dielectric materials were used to obtain an improved B_1 homogeneity and/or sensitivity profile, however, no consideration of the SNR for the entire coil was made. Additionally, some authors have demonstrated that the entire RF resonator can be replaced by a dielectric cavity [9].

Here, we concentrate on the effect that the dielectric material has on the SNR and magnetic field strength in the examined sample. For optimal performance the electric field zero at the center of the sample. Away from the center the E-field is growing while encircling the magnetic flux (as required by the Faraday law). Suboptimal E-field distributions are characterized by wobbly field lines, which are visible in simulated results and lead to excessive E-field values, and consequently higher losses and noise. The non-smooth field behavior is caused, for example, by various discontinuities such as the feed points and capacitors in coils. The preliminary rational for employing dielectric inserts stems from the observation that the electric field tends to concentrate inside materials with high dielectric constant. As will be demonstrated below, the dielectric envelope surrounding a sample facilitates smoother circulation of the electric field around it, while enhancing the magnitude of B_1 inside. It should be noted that the use of dielectric materials for improving the B_1/E ratio has been briefly described in [10].

The importance of proper field distribution has been demonstrated in Ref. [11], where an electromagnetic model has been developed in order to predict the optimal field distributions. We will present here a simpler model, which is probably less accurate, but as we will show provides accurate enough predictions for typical NMR spectroscopy cases. This approach will allow us to derive a very simple analytic formula for the maximal *IFR*, while later on we demonstrate the effect of various dielectric envelopes on the field patterns. The SNR improvement due to the dielectric envelope results from a larger increase in B_1 than in E in the region of interest. Fortunately, B_1 homogeneity within this region is barely affected by this intervention.

2. Estimating the maximal *IFR* in spectroscopy for cylindrical samples

In this section, a theoretical model is presented for the prediction of the maximal *IFR* obtainable from a given loaded volume coil. Towards studying volume coils for spectroscopy, we model the sample by a long dielectric cylinder of radius a and length L along the z-axis, immersed in a nearly homogenous y-directed magnetic field. To keep the model simple, it is assumed that the sample conductivity is uniform. The fields in the homogeneous cylindrical structure, excited by a cosinusoidal z-directed surface current $J_s(\rho = b, \varphi) = \cos(\varphi)$, enclosed by a perfectly conducting shell of radius $\rho = c$ (see Fig. 1), are given by closed form analytic expressions [12] (pp. 213–215):

$$E_z(\rho, \varphi) = AJ_1(k_d\rho)\cos\varphi \qquad (5a)$$

$$B_\varphi(\rho, \varphi) = A\frac{ik_d}{\omega}J_1'(k_d\rho)\cos\varphi \qquad (5b)$$

$$B_\rho(\rho, \varphi) = A\frac{i}{\omega\rho}J_1(k_d\rho)\sin\varphi \qquad (5c)$$

where k_d is the wave-number inside the dielectric medium ($k_d = \sqrt{\varepsilon_r}2\pi/\lambda$ with ε_r being the relative dielectric constant), ω is the angular frequency, J_n is the Bessel function of order n, J_n' is the first derivative of the pertinent Bessel function, and A is a constant depending on the problem geometry. We are assuming that all fields have a harmonic time dependence, $e^{-i\omega t}$. Though, the above fields are correct only for an infinitely long structure, we will assume that the fields remain almost the same, for a finite length cylinder (as long as its length is greater than its radius by roughly an order of magnitude). Under this assumption, we can calculate the *IFR* for a finite cylinder of radius a and length L:

$$IFR_{cyl} = \frac{\frac{\sqrt{\pi L}}{\omega} \int_0^a (k_d J_0(k_d\rho))\rho \, d\rho}{\sqrt{\sigma \frac{a^2}{2} \cdot \left(J_1'^2(k_d a) + \left(1 - \frac{1}{k_d^2 a^2} \right) J_1^2(k_d a) \right)}} \qquad (6)$$

Since in this case, the integral has to be solved numerically, Fig. 2 presents the variation of IFR_{cyl} vs. frequency for three different cylinders with various lengths (14, 35, and 175 mm). For all cylinders, the length, L, is seven times greater than the radius, a. It can be seen that the longer cylinders have higher *IFR* relative to the shorter ones. Examination of equal length cylinder for different radii has shown that changing the radius barely affects *IFR* in spectroscopy. From Fig. 2 it also can be seen that IFR_{cyl} decreases with ω. However, we must remember that this figure demonstrates only the dependence of the SNR on the electromagnetic field, and not the total SNR, which increases with ω.
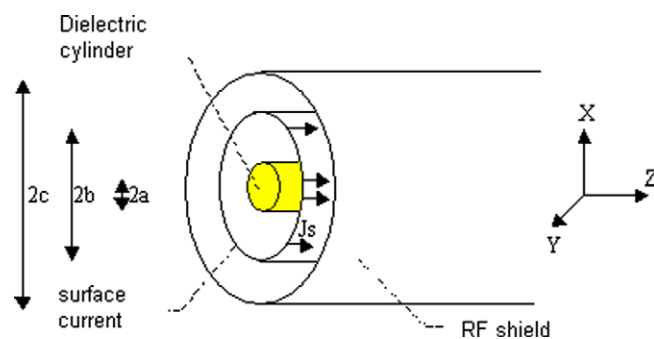

Fig. 1. Long dielectric cylinder of radius a and length L along the z-axis, immersed in a nearly homogeneous y-directed magnetic field. The homogeneous cylindrical structure is excited by a cosinusoidal z-directed surface current and enclosed by a conducting shell.
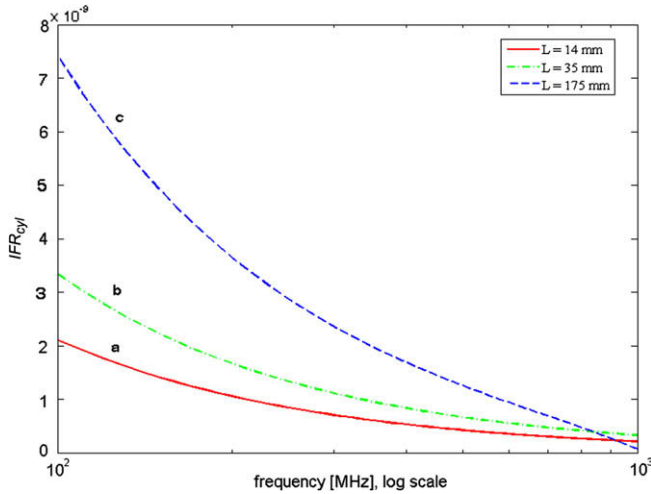
Fig. 2. IFR_{cyl} as a function of frequency for three different cylinder lengths: (a) 14, (b) 35, and (c) 175 mm.

Since the integral in (6) cannot be performed analytically, we turn to a quasistatic approximation for obtaining a simpler model. This approximation assumes that the volume of interest is very close to the z-axis, relative to the wavelength, i.e., $k_d a \ll 1$. Therefore, we get from (5):

$$E_z(\rho, \varphi) = A \frac{k_d \rho}{2} \cos \varphi \quad (7a)$$

$$B_y(\rho, \varphi) = A \frac{i k_d}{2\omega} \quad (7b)$$

This means that in the quasistatic limit we get a homogeneous magnetic field and an electric field that has a linear radial dependence.

Now, we can calculate the IFR in the quasistatic limit:

$$IFR_{cyl}^{QS} = \frac{2}{\omega} \sqrt{\frac{\pi L}{\sigma}} \quad (8)$$

This expression is a convenient result that enables us to obtain useful estimates for the IFR for cylindrical samples, under the assumptions that the fields' patterns are similar to those assumed by our analytical model given that the cylinders are sufficiently long relative to their radii.

3. Numerical simulations

Numerical simulations were performed using HFSS (version 10) software by Ansoft. All volume coils were driven by lumped voltage sources and the circuit was tuned to the relevant resonance frequency by tuning all the capacitors. Due to the use of a lumped voltage source, there is no need to match these circuits, since the ratio between the magnetic and electric fields is unaffected by a mismatch (i.e., remains the same as in the power source case). In all cases, following the introduction of the dielectric layer into the simulation, the coil was re-tuned to the original operating frequency and tested for the excitation of a single current mode yielding the desired homogenous B_1 pattern. Two coil types have been studied to verify the estimates presented in the previous section and the improvement achieved by using the dielectric envelopes.

3.1. Birdcage coil

The first simulation presented is that of an 8-leg lowpass birdcage operating at 8.4 T (360 MHz) and fed by a voltage source located at the center of one of the legs. The coil stands 40 mm high and its diameter is 38 mm. The effect of the DC coil of the scanner is modeled by a cylindrical conducting surface, 54 mm in diameter and 80 mm long. The coil is loaded by a cylindrical sample of resistive alcohol ($\varepsilon_r \approx 22$, $\sigma \approx 0.1$ S/m), 10 mm in diameter, as the examined tube. Two different models were simulated – one with a tube of 10 mm in length, and the other – 40 mm (Fig. 3). It should be noted here that the shorter cylinder does not heavily load the coil (the Q factor of the empty coil and of the coil with the short cylinder was about 60, while it was about 36 for the long tube case). Yet, our simulations show that in both cases the field pattern inside the coil is changed due to the insertion of the tubes. We will emphasize that even though the coil is not heavily loaded by the short cylinder, thus our assumption that the main losses are caused by the dielectric sample is not accurate, we still present this case as a study case since it demonstrates very well the manipulation of the electric field and the efficiency of the dielectric envelope.

The IFR_{cyl} and IFR_{cyl}^{QS} were calculated for the long tube case (Table 1) and they predict the upper bounds of 9.883×10^{-10} and 9.911×10^{-10}, respectively. The actual IFR computed using the fields simulated for this model (shown in the upper part of Fig. 4) is 8.86×10^{-10}. As long as $IFR < IFR_{cyl}$, incentive exists for improving the IFR. Here, we seek an IFR improvement by streamlining the circulation of the electric field around the sample, thus
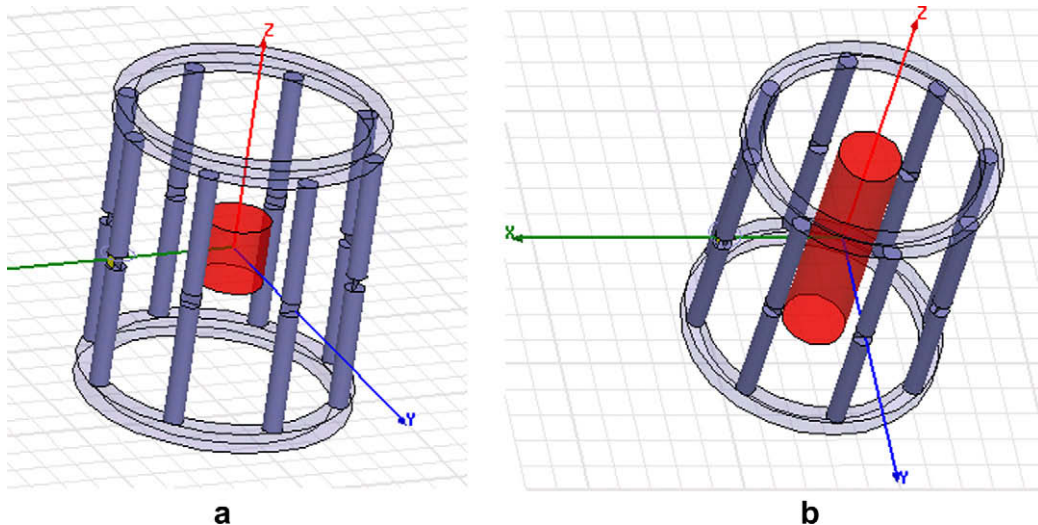

Fig. 3. An HFSS model of 8-leg lowpass birdcage operating at 8.4 T. The coil was simulated with two different cylindrical loads, both are 10 mm in diameter and length of: (a) 10, (b) 40 mm.

Table 1
IFR improvement for a 360 MHz birdcage produced by a cylindrical envelope with $\varepsilon_r \approx 80$. IFR_D and IFR_0 denote the *IFR* of the sample with and without the dielectric envelope, respectively.

Case description		Short tube: $D = 10$ mm, $H = 10$ mm	Long tube: $D = 10$ mm, $H = 40$ mm	Increased radius tube: $D = 30$ mm, $H = 40$ mm
Analytic model	IFR_{cyl}	4.939×10^{-10}	9.883×10^{-10}	9.883×10^{-10}
	IFR_{cyl}^{QS}	4.955×10^{-10}	9.911×10^{-10}	9.911×10^{-10}
No dielectric envelope	IFR_0	5.56×10^{-10}	8.86×10^{-10}	9.29×10^{-10}
	Homogeneity (%)	84	75	66
With dielectric envelope: $R_a = 6$ mm, $R_b = 16.5$ mm	IFR_D	6.67×10^{-10}	9.45×10^{-10}	–
	Homogeneity (%)	84	75	–
SNR Improvement: IFR_D/IFR_0		1.2	1.07	–

producing the magnetic field more efficiently. A manipulation of the E-field is performed by introducing a cylindrical dielectric shell into the space around the tube. The dielectric envelope (with $\varepsilon_r \approx 80$) used in the simulation has an inner radius of 6 mm and an outer radius of 16.5 mm, which leaves a 3 mm gap around the alcohol (for the test tube's material, for example). The height of the envelope is 40 mm. Following its introduction, the circulation of *E* is significantly increased (Fig. 4d), producing a stronger magnetic field. The improvement in the field pattern is reflected in

an increase in the *IFR* to 9.45×10^{-10}, which is quite close the analytic predictions, while leaving space for further optimization. For example, changing the an inner radius to 8 mm raises the *IFR* to 9.89×10^{-10}, which is literally what was expected by our theoretical model. We however, consider mainly the inner radius of 6 mm, since this case has been studied experimentally.

Next, we check the influence of the dielectric envelope on the short tube. This time, the actual *IFR* calculated by the numerical simulation is 5.56×10^{-10}, where IFR_{cyl} and IFR_{cyl}^{QS} calculated for this
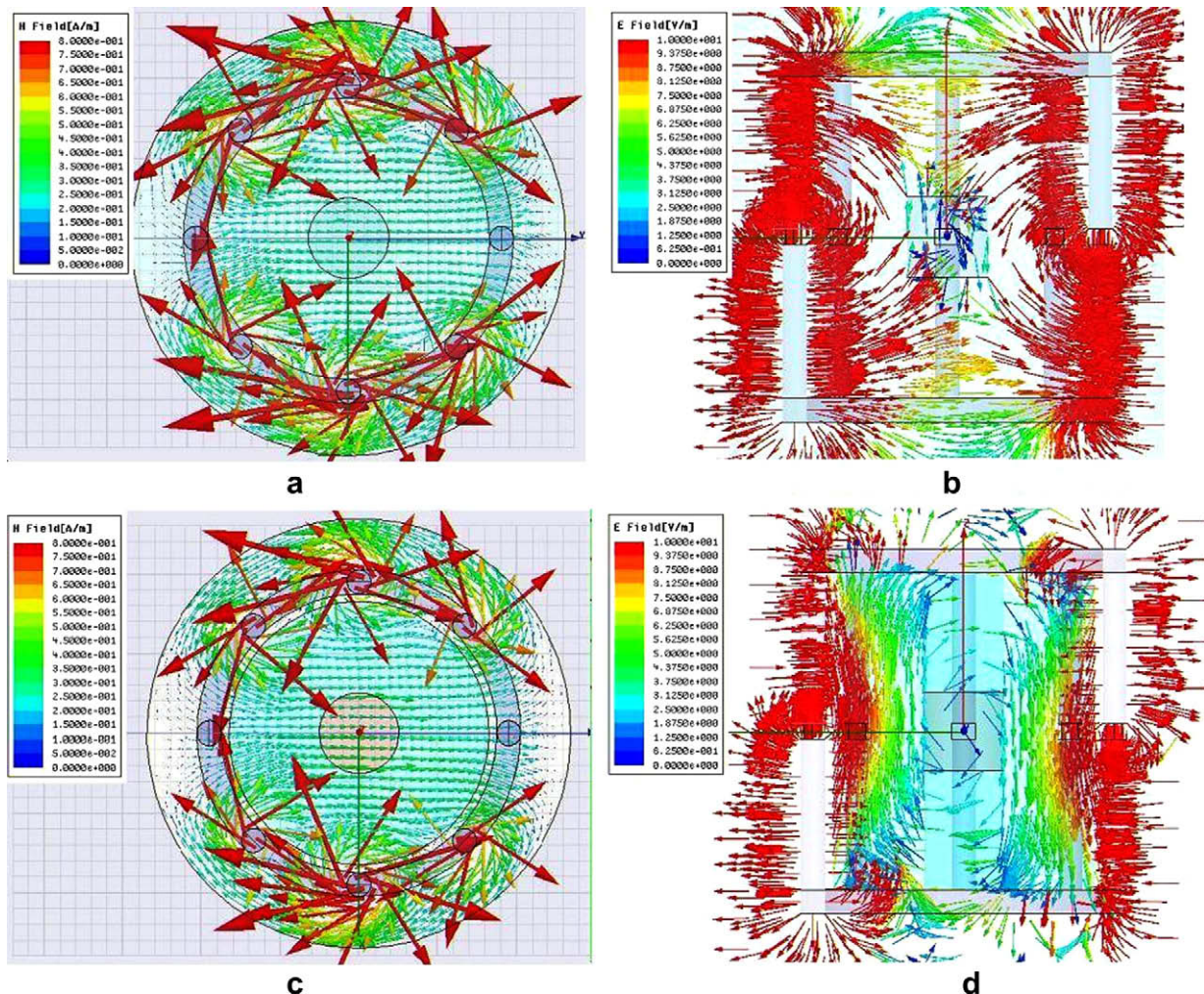

Fig. 4. Fields in the birdcage: (a) the magnetic field lines in the *x–y* plane, without the dielectric envelope, (b) the electric field lines in the *x–z* plane, without the insert, (c) the magnetic field lines in the *x–y* plane, with the dielectric envelope, (d) the electric field lines in the *x–z* plane, with the envelope – an improved circulation of the electric field is easily noticeable in this figure.
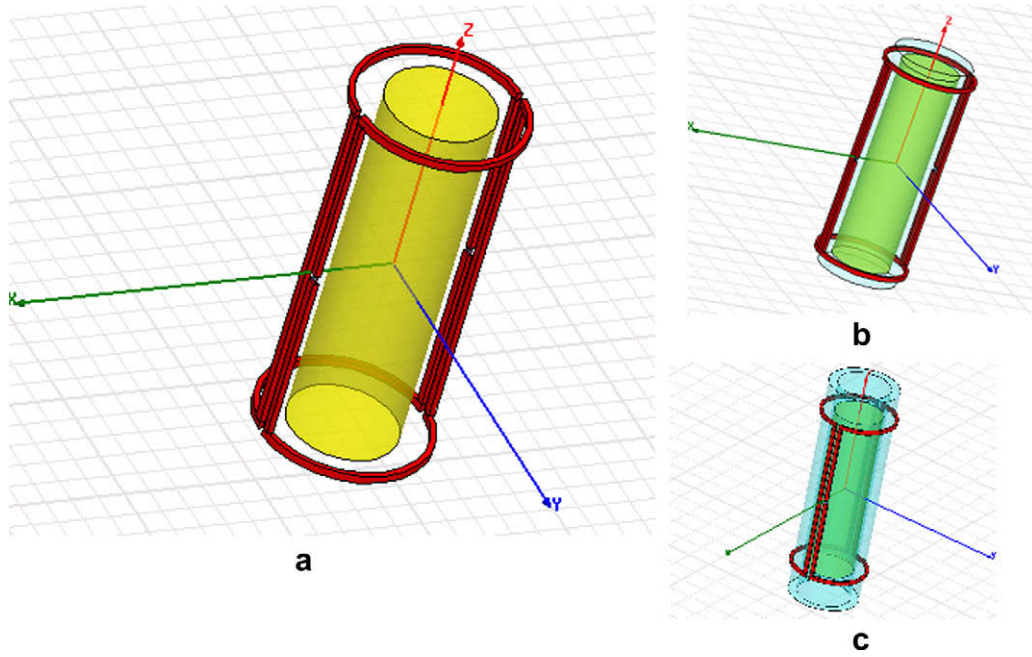
Fig. 5. A dual-feed saddle coil, with a cylindrical tube: (a) no dielectric insert; (b) with a 15.4 mm long dielectric envelope with inner and outer radii of 2 and 2.7 mm, respectively, and 0.7 mm thick upper and bottom disks caps; (c) with a 19 mm long dielectric envelope with inner and outer radii of 2.2 and 2.9 mm, respectively.

problem (Table 1) predict the upper bounds of 4.939×10^{-10} and 4.955×10^{-10}, respectively. The reason for the high value of the IFR relative to the one that is expected by the models is that these models assume that the cylinder is long relative to its diameter, which is not the case for the short tube. Therefore, the IFR might still be improved. Indeed, using a similar dielectric envelope, with an inner radius of 6 mm, and outer radius of 16.5 mm, improves the IFR to 6.67×10^{-10}. In Fig. 4d bottom, the improved circulation of E due to the dielectric insert can be easily observed.

Results for the two simulations of the birdcage loaded by the cylindrical tubes are summarized in Table 1, where R_a and R_b are the corresponding inner and outer radii of the dielectric envelope. Note that B_1 homogeneity is not affected by all of the above manipulations. In order to emphasize the improvement achieved by the dielectric envelope simulation, results for the same coil with a cylindrical sample of 30 mm in diameter and 40 mm in length were added to Table 1. As can be seen, this configuration results in a worse homogeneity relative to the narrow tube. Yet, the IFR is slightly better relative to the narrow tube, but not as good as with the dielectric envelope.

3.2. Saddle coil

In order to increase our confidence in the suggested method, we will apply it to another volume coil – a saddle coil, and at a different frequency – 900 MHz. The coil stands 14 mm high and its diameter is 6 mm. The effect of the DC coil of the scanner is modeled by a cylindrical conducting surface, 40 mm in diameter and 20 mm long. The coil is fed on both sides (in order to produce sym-

metric fields), and loaded by a cylindrical sample of a compound of resistive saline ($\varepsilon_r, \sigma \approx 50$ S/m), 4 mm in diameter with a length of 14 mm (Fig. 5a).

The IFR_{cyl} and IFR_{cyl}^{QS} calculated for this problem (see Table 2) predict the upper bounds of 10.07×10^{-11} and 10.48×10^{-11}, respectively, while the actual IFR obtained via the fields simulated for this model (Fig. 6a and c) is 9.57×10^{-11}. Again, since $IFR < IFR_{cyl}$ we surmise that we can improve the IFR. Therefore, dielectric envelopes with inner and outer radii of 2 and 2.7 mm, respectively, surrounding the sample cylinder (see Fig. 5b), with a height of 15.4 mm (including 0.7 mm thick upper and lower end disks) and with different dielectric constants (ranging from $\varepsilon_r = 140$ up to $\sigma_r = 300$ were used in order to enhance the circulation of the electric field. The reason for the very high dielectric constant is that the spacing available for the dielectric envelope (0.7 mm) is very thin, relative to the prescribed wavelength. This imposes the use of high dielectric constant material in order to compensate for the small thickness of the envelope.

The corresponding IFR obtained for the tube coated with a material with $\sigma_r = 300$ is 10.62×10^{-11} (Fig. 6b and d).

Results for the two simulations of the saddle coil loaded by the cylindrical tube are summarized in Table 2. Note that once again B_1 homogeneity is hardly affected by all of the above manipulations. Also in this table we added the results of the alternative option – a sample occupying the whole available volume: 5.4 mm in diameter and a length of 14 mm. In this case, both the homogeneity and the IFR are worse than those of all the other cases. Note that the envelope design is quite robust and non unique. For example, a slightly higher improvement (1.12, instead of 1.11 as in the best

Table 2
IFR improvement for a 900 MHz saddle coil with dual feed.

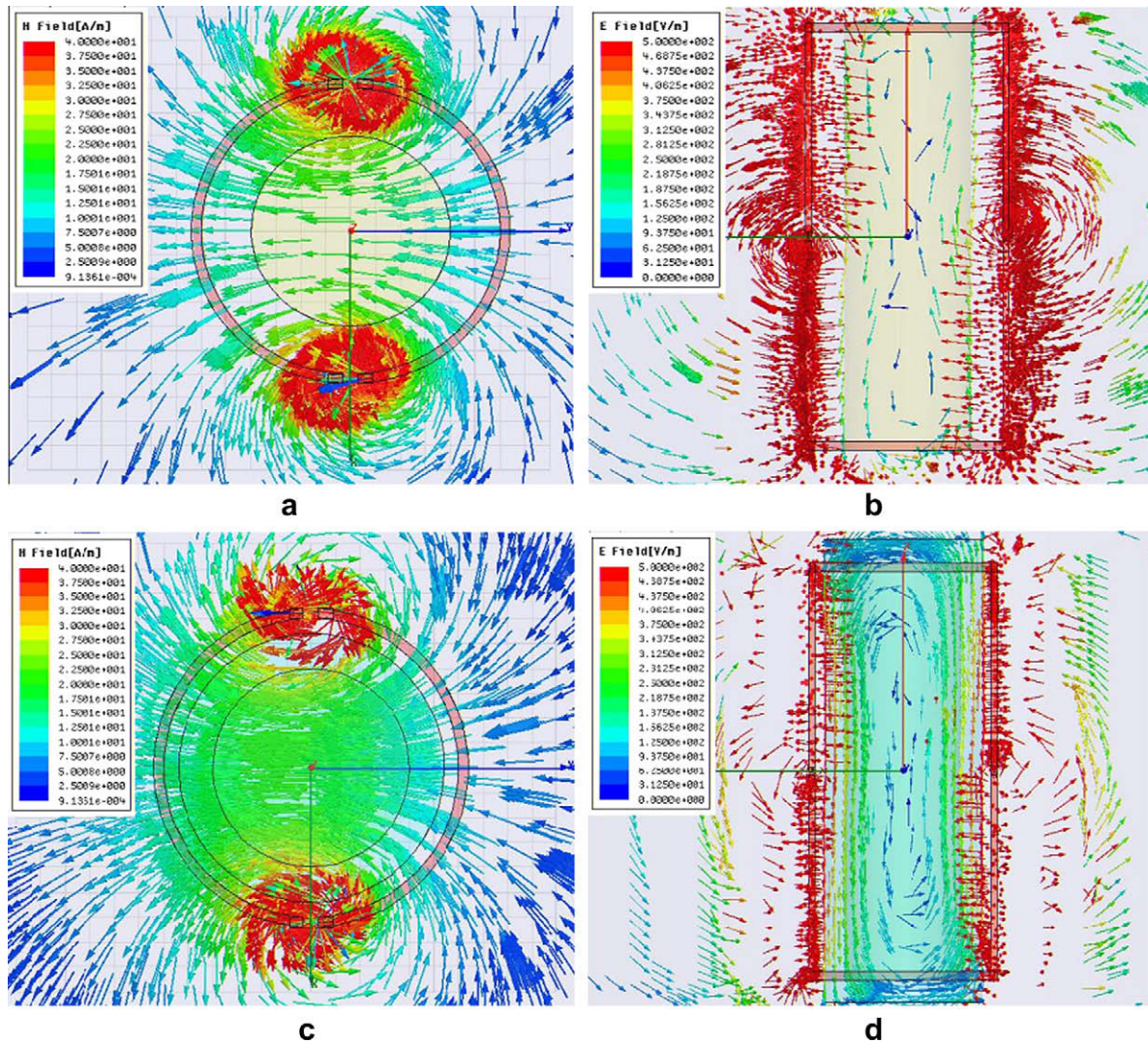| Case description	IFR_0	$\frac{IFR_{cyl}}{IFR_0}$	$\frac{IFR_{cyl}^{QS}}{IFR_0}$	$\frac{IFR_D}{IFR_0}$			Homogeneity (%)
				$\varepsilon_r = 140$	$\varepsilon_r = 200$	$\varepsilon_r = 300$	
Sample diameter: $D = 4$ mm	9.57×10^{-11}	1.052	1.095	1.042	1.078	1.11	69
Sample diameter: $D = 5.4$ mm	$9.06 \cdot 10^{-11}$	1.11	1.156	–	–	–	60

Fig. 6. Fields in a dual-feed saddle coil: (a) the magnetic field lines in the x–y plane, without the dielectric insert, (b) the electric field lines in the x–z plane, without the dielectric envelope, as described in Fig. 5a, (c) the magnetic field lines in the x–y plane, with the dielectric insert, (d) the electric field lines in the x–z plane, with the dielectric envelope, as described in Fig. 5b.

case of the previous envelope) is achieved when the dielectric envelope has inner and outer radii of 2.2 and 2.9 mm, respectively, with a length of 19 mm (Fig. 5c).

4. Experimental

An experiment was designed in order to put the results of our theoretical model and numerical simulations to the test of reality with regard to the enhancement of the SNR and B_1. A wide bore 360 MHz Bruker AVANCE NMR spectrometer was used. The coil was an 8-leg shielded linear birdcage by Bruker. A cylindrical phantom with two compartments was inserted into the internal bore of the coil (Fig. 7), where the inner cylinder (1 cm in diameter, 1 cm high) was filled with resistive alcohol ($\varepsilon_r \approx 22$, $\sigma \approx 0.1$ S/m). The external cylinder (1.2 cm inner diameter, 3.4 cm outer diameter, 6.5 cm height) was empty in the first step and was filled with D_2O ($\varepsilon_r \approx 78$) in the second step. D_2O has no NMR resonance at 360 MHz so that NMR signal was only obtained from the alcohol compartment located in the middle of the phantom, while the external layer served as a dielectric envelope for the sample volume. The two main reasons for designing a small sample compartment were: (a) to enable measurement of B_1 over a volume where

it is homogenous; (b) to leave a sufficient space for a thick dielectric envelope that can provide a significant effect on the SNR, given
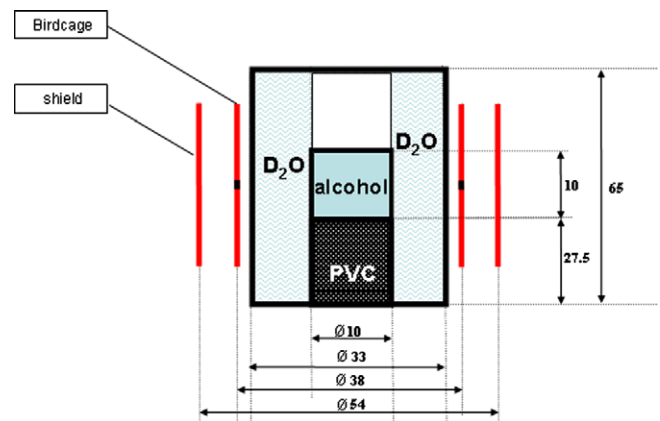

Fig. 7. A schematic of the cylindrical phantom which was used in the experiment: the inner compartment was filled with alcohol; the outer compartment was filled with D_2O and was used as a dielectric envelope.

the dielectric envelope material (D_2O with $\varepsilon_r \approx 78$) and the small ratio of the coil size to the wavelength (almost 1 to 30). Alternatively, a higher ε_r material would be needed.

The same receiver gain was used in both steps (without and with the dielectric envelope) while tuning and matching were carefully adjusted. In both steps, ω_1 ($\omega_1 = 2\pi/T$, where T is the pulse duration) was calculated from the results of a single-pulse spectroscopic measurement of the signal amplitude as a function of the pulse length. Results were fitted to a sine to obtain $\omega_1 = 19900$ rad/s for the first step and $\omega_1 = 23300$ rad/s for the second step (with the D_2O dielectric envelope), indicating B_1 amplification by a factor of 1.16. This figure is in good agreement with the HFSS simulation, which predicts the same B_1 amplification (see first row in Table 3).

In order to quantify the SNR under the same conditions for both steps, the alcohol spectrum was obtained using the pulse length that gave maximum signal amplitude in each case (80 μs without and 70 μs with the dielectric envelope). Signal amplitude was measured in two ways: by the intensity of the biggest methyl peak and by taking the integral of the entire methyl triplet. The latter method was adopted to account for the line width differences between the two experiments. Noise was measured away from the peaks within a 5 ppm range, using an SNR function (SINO) by Bruker. Despite the baseline correction, the choice of the frequency range in which the noise is measured has a critical effect on the measured noise levels. The SNR improvement between the second step and the first step was 1.208 when the signal corresponds to the height of the highest methyl peak, while when the signal measurement was based on the integral of the entire methyl triplet the improvement was 1.24. The simulation predicts that the improvement is 1.2. We must emphasize here that all the *IFR* values and expressions given above are relative to the *voltage* SNR. For the sake of uniformity, the measured improvement in *power* SNR (which is a square of the voltage SNR ratio) was converted to *voltage* SNR.

The same two step experiment was repeated, this time, with a 40 mm long tube of alcohol, and the same dielectric envelope as above. The B_1 enhancement and SNR improvement were also measured in the same way as above. Results from the described experiments and corresponding simulations are summarized in Table 3. The good agreement between the simulations and experiments validates the numerical simulations and, therefore, supports the predictions of the theoretical model for the upper bound, IFR_{cyl}, as presented above.

5. Conclusions

A method for the improved design and upgrading of volume coils was presented and shown to enhance both transmitted magnetic field and SNR without any observable effect on B_1 homogeneity. The SNR is improved by manipulating the circulation of E within the coil by introducing dielectric inserts with cylindrical symmetry so that the circulation of E becomes smoother and thereby producing the magnetic field more efficiently. Another effect of the improved circulation of E is that the resultant increased magnitude of B_1 can be translated into either shorter pulses or lower required transmission power. Alternately, the presented improvement allows us to use a shorter tube, since the *IFR* and therefore the SNR is proportional to the tube length, while keeping the same threshold of detection.

Table 3
Comparison of the SNR and B_1 enhancement between the HFSS simulations and experiment performed on a 8.4 T mini-MRI system.

		Voltage SNR improvement	B_1 enhancement
10 mm tube length	Simulation	1.2	1.16
	Experiment	1.208–1.24	1.16
40 mm tube length	Simulation	1.07	1.13
	Experiment	1.035–1.081	1.12

A simple theoretical model for predicting the upper bound for the *IFR* under optimal conditions was presented. By reducing this model to the quasistatic regime, a simple analytic formula can be obtained for the *IFR* (IFR_{cyl}). The model proved to be highly accurate in predicting the *IFR* over a wide range of frequencies and sample sizes. Simulation results throughout this work and, therefore, prediction of the theoretical model are supported by experimental measurements performed on a mini-scale MRI system operating at 8.4 T with a shielded birdcage coil. Measured parameters like B_1 enhancement and increase in the SNR produced by the addition of the dielectric layer are in very good correlation with those predicted by the simulations.

Using a tube with a smaller diameter, which in the QS limit is not affecting the maximal *IFR* (IFR_{cyl}^{QS}), allows the use of a thicker envelope layer. This enables using a material with a lower dielectric constant, or even leads to a further improvement of the *IFR*. The dielectric inserts can be used whenever a manipulation of the electric field is needed, in order to achieve an optimal field. For example, as shown in this work, one can improve the circulation of the electric field inside the examined sample. In addition, the asymmetry, if exists, of the field in the sample itself can be corrected.

References

[1] D.I. Hoult, R.E. Richards, The signal-to-noise ratio of the nuclear magnetic resonance experiment, J. Magn. Reson. 24 (1976) 71.
[2] D.I. Hoult, P.C. Lauterbur, The sensitivity of the zeugmatographic experiment involving human samples, J. Magn. Reson. 34 (1979) 425.
[3] D.I. Hoult, B. Bhakar, NMR Signal, Reception: virtual photons and coherent spontaneous emission, Concepts Magn. Res. 9 (1998) 277–297.
[4] T.K.F. Foo, C.E. Hayes, Y.W. Kang, An analytical model for the design of RF resonators for MR body imaging, Magn. Reson. Med. 21 (1991) 165–177.
[5] E.J. Butterworth, E.G. Walsh, J.W. Hugg, A TiO_2 dielectric filled toroidal radio frequency cavity resonator for high-field NMR, NMR Biomed. 14 (2001) 184–191.
[6] W. Renz, High-frequency system for nuclear spin tomography with shield for delimitation of an electric field. US Patent 5410251, 1995.
[7] Q.X. Yang, M.B. Smith, H. Liu, X. Zhang, J. Wang, K. Ugurbil, W. Chen, Manipulation of signal intensity distribution with dielectric loading at 7.0 T, Proc. Int. Soc. Mag. Reson. Med. 9 (2001) 1096.
[8] M. Sreenivas, M. Lowry, C. Tan, M.D. Pickles, P. Gibbs, L.W. Turnbull, A simple solution for reducing the dielectric artifact in clinical MR imaging at 3 T, Proc. Int. Soc. Mag. Reson. Med. 11 (2005) 2754.
[9] H. Wen, F.A. Jaffer, T.J. Denison, S. Duewell, A.S. Chesnick, R.S. Balaban, The Evaluation, The evaluation of dielectric resonators containing H_2O or D_2O as RF coils for high-field MR imaging and spectroscopy, J. Magn. Res. Ser. B 110 (1996) 117–123.
[10] L.A. Crum, K.W. Zilm, Resonator designs for decreasing sample heating in solid state NMR experiments, in: Proceedings of the Experimental Nuclear Magnetic Resonance Conference on 48th ENC, 2007.
[11] T.M. de Swiet, Optimal electric fields for different sample shapes in high resolution NMR spectroscopy, J. Magn. Res. 174 (2005) 331–334.
[12] J. Jin, Electromagnetic Analysis and Design in Magnetic Resonance Imaging, CRC Press Series in Biomedical Engineering, Boca Raton, FL, 1999.